Fathoming the anisotropic magnetoelasticity and magnetocaloric effect in GdNi

B. P. Alho, P. O. Ribeiro, V. S. R. de Sousa, B. C. Margato, Anis Biswas, Tyler Del Rose, R. S. de Oliveira, E. P. Nóbrega, P. J. von Ranke, Y. Mudryk, and V. K. Pecharsky

Fathoming anisotropic magnetoelasticity and magnetocaloric effect of GdNi

B. P. Alho[1], P. O. Ribeiro[1], V. S. R. de Sousa[1], B. C. Margato[1], Anis Biswas[2], Tyler Del Rose[2,3], R. S. de Oliveira[1], E. P. Nóbrega[1], P. J. von Ranke[1], Y. Mudryk[2], V.K. Pecharsky[2,3]

[1] Instituto de Física, Universidade do Estado do Rio de Janeiro - UERJ, Rua São Francisco Xavier, 524, 20550-013, RJ, Brazil.

[2] The Ames National Laboratory, U.S. Department of Energy, Iowa State University, Ames, IA, 50011-3020, USA

[3] Department of Materials Science and Engineering, Iowa State University, Ames, IA, 50011-2300, USA

Corresponding Author: B. P. Alho

Universidade do Estado do Rio de Janeiro, IF - DEQ

Rua São Francisco Xavier, 524 - 3^0 andar.

Maracanã - Rio de Janeiro – 20550-013, Brazil.

E-mail: brunoalho@gmail.com

Abstract

Intermetallic GdNi adopts a CrB type of crystal structure (space group *Cmcm*), and it orders ferromagnetically via a second-order phase transition at 70 K, exhibiting unusually strong spontaneous striction along the three independent crystallographic axes in the ferromagnetically-ordered state. We introduce a new microscopic model to describe anisotropic changes of lattice parameters and elastic contribution to magnetocaloric effect of GdNi. In the model, results of DFT calculations are used as inputs into a Hamiltonian that includes elastic energy of an anisotropic crystal lattice, exchange interactions, and Zeeman effect. The magnetic and elastic Hamiltonians are coupled through an anisotropic Bean – Rodbell model of magnetoelastic interactions. This coupling gives rise to anisotropic changes in the lattice parameters observed experimentally, and the model reveals good to reasonable agreements between the current theoretical results and earlier experimental data, thus validating the model within the limits of assumptions made. We also show that DFT calculations with $4f$ electrons of Gd treated as core electrons lead to a more adequate estimate of elastic constants of GdNi in comparison with the LDA + U method where $4f$ electrons are treated as valence electrons.

1. Introduction

Rare earth-based intermetallic compounds are of interest to condensed matter scientists due to a broad spectrum of fundamentally interesting physical and chemical phenomena that are, at the same time, technologically significant, such as unconventional superconductivity, hard magnetism, giant magnetocaloric effects (GMCEs), quantum criticality, anhysteretic first-order phase transitions, large magnetic anisotropies, catalytic behaviors, and many other [1–8]. Several of those phenomena originate from strong coupling of crystal lattices with large localized $4f$ magnetic moments, characteristic of lanthanides, through magnetoelastic interactions. For example, magnetocaloric effects, quantified as the isothermal entropy change (ΔS_T) or/and the adiabatic temperature change (ΔT_S), may reach outstanding values when magnetoelastic interactions are strong. A notable representative is $Gd_5Si_2Ge_2$ [3], where near room temperature ΔS_T = -14 J Kg^{-1} K^{-1} for ΔH = 20 kOe is 2.5 times higher than that of elemental Gd for the same magnetic field change due to a discontinuous magnetostructural phase transition that occurs in the former, giving rise to GMCE.

In recent years, the magnetoelastic coupling and its role in the evolution of phase transformations has been investigated in a number of compounds both experimentally and theoretically. Alvaranega *et al.* [9] examined the first-order magnetic phase transition of $Gd_5Si_2Ge_2$ using a microscopic model based on the Bean-Rodbell [10] approach. The anhysteretic first-order phase transition of Eu_2In, with a very small volume change of about 0.1%, has been studied experimentally and theoretically from first-principles [5, 11], and using a mean-field model that takes into account magnetoelastic coupling [12]. Second-order phase transitions in GdNi [13] and $GdNiSi_3$ [14], where anisotropic changes in lattice constants occur in the vicinities of global magnetic ordering transitions, have been probed as well.

Among different rare earth-based materials, only a few intermetallic compounds exhibit rather unconventional second-order magnetic phase transition with concurrent changes in both magnetism and crystallographic lattice, while crystal symmetry remains invariant across phase boundaries. One of the prime examples of those is GdNi, which shows anisotropic changes in crystallographic parameters during

its second-order magnetic phase transition at $T_C \sim 71$ K. The transition is iso-symmetric magnetoelastic, and it gives rise to an appreciably large, tunable with Co-doping magnetocaloric effect [14]. Here, magnetoelastic coupling plays an important role in the development of interesting thermomagnetic properties of $GdNi_{1-x}Co_x$, albeit the compounds exhibit second-order magnetic phase transitions irrespective of x_{Co} [15].

Although the mean-field approach has been successfully applied to describe magnetoelastic coupling in many materials, there is significant room for improvements. For example, there are new experimental results that cannot be described with previously established models, such as the anisotropic, temperature-dependent spontaneous striction in the case of GdNi below its Curie temperature (T_C) [13]. While earlier models employed to describe volume changes using magnetoelastic coupling consider isotropic magnetoelastic interactions, they do not allow to calculate the lattice parameters independently. To bring light to this subject we propose a new microscopic model, which includes exchange interactions coupled to the elastic energy through anisotropic magnetoelastic interactions. This model is then used to investigate the magnetic and thermal properties of GdNi, including the temperature-dependent anisotropic changes of lattice parameters observed experimentally.

2. **Theory**

GdNi crystallizes in the orthorhombic CrB-type structure and orders ferromagnetically at a T_C around 70 K [13,16,17]. In order to describe its magnetic and elastic properties, the model Hamiltonian is composed of a magnetic contribution, $\mathcal{H}_{mag}$, from the $4f$ electrons of Gd^{3+} ions, neglecting the Ni ions, which are non-magnetic [5,13], and an elastic term, $\mathcal{H}_{el}$:

$$\mathcal{H} = \mathcal{H}_{mag} + \mathcal{H}_{el}, \tag{1}$$

where

$$\mathcal{H}_{mag} = \sum_{i,\, l,m} \mathfrak{J}_{i,lm} J_l^i J_m^i - g\mu_B \mu_0 \sum_{i,l} H_i J_l^i, \tag{2}$$

and

$$\mathcal{H}_{el} = \frac{V_0}{2} \sum_{\alpha,\delta} C_{\alpha\delta} \varepsilon_\alpha \varepsilon_\delta. \tag{3}$$

4

The first term in the Hamiltonian (2) represents exchange interactions between Gd ions, where $\mathfrak{I}_{i,lm}$ are the exchange parameters, J_l^i represent the i-th Cartesian component of the total magnetic moment of the Gd ions and the sums l, m are taken over all magnetic ions. The second term in (2) represents the Zeeman effect, where g is the Landè factor, μ_B is the Bohr magneton, and $\mu_0 H_i$ is the i-th component of the applied magnetic field. Hamiltonian (3) represents the elastic energy, where V_0 is the unit cell volume at a reference temperature, $C_{\alpha\delta}$ are the stiffness constants, with $\alpha, \delta = 1, \dots, 6$ following the generalized Hooke's law in the Voigt notation [18,19], which is given by $\sigma_\alpha = \sum_\delta C_{\alpha\delta}\varepsilon_\delta$, where σ_α and ε_δ are the stress and strain components, respectively. It is worth noting that, in general, there are 21 independent stiffness constants, number of which is reduced as crystal symmetry increases from triclinic to cubic. For the orthorhombic CrB-type structure of GdNi there are 9 independent stiffness constants [20].

Equation (2) can be simplified considering a mean field approximation, and the average among nearest-neighbor exchange interactions considering that all of the Gd ions in the structure are crystallographically equivalent, leading to $\mathfrak{I}_{i,lm} = \mathfrak{I}_i$. In this framework, the exchange term, per ion, can be written as:

$$\sum_{i,\,l,m} \mathfrak{I}_i J_l^i J_m^i \xrightarrow{per\ ion} \sum_i \lambda_i \langle J^i \rangle J^i + \frac{\lambda_i \langle J^i \rangle^2}{2}, \tag{4}$$

where $\lambda_i = 2z\mathfrak{I}_i$ are the normalized exchange parameters, z is the number of nearest neighbors and $\langle J^i \rangle$ is the thermodynamic mean of the i-th component of the total magnetic moment.

In order to couple the magnetic and elastic Hamiltonians, we consider an anisotropic Bean – Rodbell-like [10,21] dependency of the normalized exchange parameters, given by:

$$\lambda_i = \lambda_{i0} + \lambda_{i1}\varepsilon_i, \tag{5}$$

where λ_{i0} are the exchange parameters without strain, λ_{i1} are the magnetoelastic parameters, and ε_i are the first three strain components, with i = 1, 2 and 3. Coupling of the exchange parameters with only the three first strain components avoids monoclinic or triclinic distortions since GdNi remains orthorhombic at any temperature [13]. From here on we, therefore, consider $\varepsilon_4 = \varepsilon_5 = \varepsilon_6 = 0$.

Combining equations (2) through (5) in the total Hamiltonian (1), after normalization to a single ion the eigenvalues and eigenvectors can be obtained, and the Helmholtz free energy can be calculated as:

$$F = f - k_B T ln\left[\frac{sinh\left[\left(\frac{2J+1}{2J}\right)x\right]}{sinh\left[\left(\frac{1}{2J}\right)x\right]}\right],$$ (6)

where $f = \frac{1}{2}\sum_i \lambda_i \langle J^i \rangle^2 + \mathcal{H}_{el}$, $x = \beta|\vec{H}^{ef}|J$, $\beta = \frac{1}{k_B T}$, k_B is the Boltzmann constant, T is the temperature, $\vec{H}^{ef}$ is the effective magnetic field with $H_i^{ef} = \lambda_i \langle J^i \rangle + g\mu_B \mu_0 H_i$ being its components. The order parameters in equation (6) are the three mean values of the total magnetic moment components, $\langle J^i \rangle$, which are associated with the magnetization through $M_i = g\mu_B \langle J^i \rangle$, and the 6 strain components, ε_α, as described below. By minimizing the Helmholtz free energy with respect to each of the nine order parameters, one obtains for $\langle J^i \rangle$:

$$\langle J^i \rangle = J \frac{H_i^{ef} B_J(x)}{|\vec{H}^{ef}|},$$ (7)

where $B_J(x)$ is the Brillouin function and for ε_α:

$$\varepsilon_1 = \frac{(C_{22}C_{33}-C_{23}{}^2)\lambda_{11}\langle J^1 \rangle^2 + (C_{23}C_{13}-C_{33}C_{12})\lambda_{21}\langle J^2 \rangle^2 + (C_{12}C_{23}-C_{22}C_{13})\lambda_{31}\langle J^3 \rangle^2}{C},$$ (8)

$$\varepsilon_2 = \frac{(C_{23}C_{13}-C_{33}C_{12})\lambda_{11}\langle J^1 \rangle^2 + (C_{11}C_{33}-C_{13}{}^2)\lambda_{21}\langle J^2 \rangle^2 + (C_{12}C_{13}-C_{11}C_{23})\lambda_{31}\langle J^3 \rangle^2}{C},$$ (9)

$$\varepsilon_3 = \frac{(C_{12}C_{23}-C_{22}C_{13})\lambda_{11}\langle J^1 \rangle^2 + (C_{12}C_{13}-C_{11}C_{23})\lambda_{21}\langle J^2 \rangle^2 + (C_{11}C_{22}-C_{12}{}^2)\lambda_{31}\langle J^3 \rangle^2}{C},$$ (10)

$$\varepsilon_4 = \varepsilon_5 = \varepsilon_6 = 0,$$ (11)

where $C = V_0(C_{11}C_{22}C_{33} - C_{33}C_{12}{}^2 - C_{11}C_{23}{}^2 - C_{22}C_{13}{}^2 + 2C_{12}C_{13}C_{23})$.

3. DFT Methods

Elastic constants were calculated using spin polarized density functional theory (DFT) as implemented in Quantum Espresso [22–24] and the thermo_pw package [25]. All calculations were performed using the recommended standard solid-state pseudopotentials (SSSP Efficiency) [26,27] for Gd [28,29] and Ni [30], employing the generalized gradient approximation of Perdew, Burke and Ernzerhof [31,32]. 4f electrons of Gd were treated using two different approaches: i) 4f as core electrons (open core approximation) and (ii)

4*f* as valence electrons. In the latter case, the placement of strongly correlated 4*f*-states was corrected by an effective Hubbard term $U_{eff} = U - J = 6$ eV as prescribed by Cococcioni and Gironcoli [33].

Geometry optimization was performed as follows. First, the experimental *b*/*a* and *c*/*a* ratios and atomic positions, are used to perform a series of energy *vs.* volume calculations in order to obtain the equilibrium volume, which is fitted to the Birch-Murnaghan [34,35] equation of state. Next, using the equilibrium volume, the b/a ratio is varied while keeping c/a fixed, fitting the resulting $E \times b/a$ data to a 4th order polynomial to obtain the equilibrium b/a; the same procedure is followed to optimize c/a. Finally, the atomic coordinates are relaxed using the optimized lattice parameters. For these calculations, we consider a 6x6x5 k-mesh, cutoff energies of 90 Ry (4*f* as core) and 60 Ry (4*f* as valence) and total energy accuracy of 10^{-8} Ry. Brillouin zone integrations were performed with a Methfessel-Paxton [36] smearing of 0.015 Ry. The optimized crystallographic parameters along with the bulk modulus (B) and its derivative (B') are listed in Table 1.

Table 1: DFT-optimized crystallographic parameters of GdNi, bulk modulus (B) and its derivative with respect to pressure (B').

Approach	Lattice parameters			Relaxed coordinate y		Volume (Å^3/ion)	B (GPa)	B'
	a (Å)	b (Å)	c (Å)	Gd	Ni			
4f as valence	3.7987	10.4118	4.1987	0.1397	0.4294	20.76	78	4.0
4f as core	3.7643	10.1294	4.2470	0.1392	0.4277	20.24	79	3.8
Experiment	3.7730	10.3189	4.2134			20.51		

The stiffness constants, C_{ij}, were calculated employing the strain-stress method as implemented in the thermo_pw package [4]. In this method, the optimized lattice is deformed by a series of strains, allowing

for atom relaxation. For the orthorhombic CrB-type structure of GdNi, we need to determine 9 independent

elastic constants, therefore, we consider the 6 strain matrices listed below.

$$\epsilon_C = \begin{pmatrix} \epsilon_1 & 0 & 0 \\ 0 & 0 & 0 \\ 0 & 0 & 0 \end{pmatrix} \qquad \epsilon_D = \begin{pmatrix} 0 & 0 & 0 \\ 0 & \epsilon_2 & 0 \\ 0 & 0 & 0 \end{pmatrix} \qquad \epsilon_E = \begin{pmatrix} 0 & 0 & 0 \\ 0 & 0 & 0 \\ 0 & 0 & \epsilon_E \end{pmatrix}$$

$$\epsilon_G = \frac{1}{2}\begin{pmatrix} 0 & \epsilon_6 & 0 \\ \epsilon_6 & 0 & 0 \\ 0 & 0 & 0 \end{pmatrix} \qquad \epsilon_H = \frac{1}{2}\begin{pmatrix} 0 & 0 & \epsilon_5 \\ 0 & 0 & 0 \\ \epsilon_5 & 0 & 0 \end{pmatrix} \qquad \epsilon_I = \frac{1}{2}\begin{pmatrix} 0 & 0 & 0 \\ 0 & 0 & \epsilon_4 \\ 0 & \epsilon_4 & 0 \end{pmatrix}$$

The application of ϵ_C, ϵ_D and ϵ_E does not change the orthorhombic cell shape, only affecting the a, b

and c lattice parameters, respectively. Conversely, ϵ_G, ϵ_H and ϵ_I lead to a monoclinic distortion.

Furthermore, ϵ_C allows the determination of C_{11}, C_{12} and C_{13}; from ϵ_D one obtains C_{22} and from ϵ_E one

obtains C_{33}. Consequently, ϵ_G, ϵ_H and ϵ_I allow the determination of C_{66}, C_{55} and C_{44}, respectively.

For each matrix, six strains are applied in the range between [-1.25%, 1.25%], so the lattice remains in

the elastic regime, resulting in 36 relaxation procedures. For these calculations we increase the k-mesh to

10x10x8 while keeping the other parameters as described above. We point out that in order to improve

convergence, we increased the number of electronic bands to 50 for 4f as core and to 60 for 4f as valence

electrons.

The calculated stiffness constants (no experimental data exist) are shown in Table 2, where set 1

corresponds to spin polarized calculations with 4f as valence and set 2 to 4f as core electrons. We note a

good agreement between the constants calculated by the two methods, showing that, as expected, 4f

electrons do not contribute significantly to bulk elastic properties. This can also be seen from the optimized

crystallographic parameters shown in Table 1, where the largest difference does not exceed 3%.

Table 2: Stiffness constants (in GPa) for GdNi crystal obtained from spin polarized GGA calculations

using the 4f as valence (set 1) and the 4f as core electrons (set 2).

	C_{11}	C_{12}	C_{13}	C_{22}	C_{23}	C_{33}	C_{44}	C_{55}	C_{66}
set 1	97	56	70	97	71	103	35	27	27
set 2	88	56	70	103	72	103	38	30	30

One may verify that both sets of stiffness constants shown in Table 2 satisfy the necessary and sufficient Born criteria for the stability of orthorhombic systems [37]. Since these constants are valid for single crystals, one may use the Voigt [18], Reuss [38] and Hill average [39] methods to determine the polycrystalline bulk modulus (B) and shear modulus (G), from which one may obtain Young's modulus (E), Poisson's ratio (ν) and also estimate the Debye temperature (θ_D) [40,41]. Thus determined constants for an isotropic polycrystalline material are listed in Table 3.

Table 3: Isotropic bulk modulus (*B*) and shear modulus (*G*) in GPa obtained from the stiffness constants (C_{ij}) using Voigt (B_V, G_V), Reuss (B_R, G_R), and Hill (B_H, G_H) average methods; Young's modulus (*E* in GPa); Poisson's ratio (ν); and Debye temperature (θ_D in K) for GdNi.

	B_V	B_R	B_H	G_V	G_R	G_H	*E*	ν	θ_D
set 1	77	77	77	24	22	23	63	0.36	199
set 2	76	70	73	26	22	24	65	0.35	202

4. Results and discussions

To describe the magnetoelastic properties of GdNi using the proposed mean-field model, we use the DFT-derived stiffness constants from Table 2. In the model, the shear stress components of equation (11) are null. Hence, C_{44}, C_{55}, C_{66} do not contribute to the calculations of the order parameters. Also, to further simplify the model we take $\lambda_{10} = \lambda_{20} = \lambda_{30} = \lambda_0$, i.e., assume isotropic exchange interactions in the absence of strain, and postulate that $\lambda_{11} = \lambda_{21} = 0$ and $\lambda_{31} \neq 0$, i.e., magnetoelastic interactions are considered only along the z-axis. We note that the latter postulation assumes the z-axis as the easy magnetization direction, which is reasonable considering that linear striction below T_C along the z-axis is opposite to that observed along the x and y axes. As illustrated in Figure 1, by considering magnetoelastic interactions exclusively along the z-axis, the model predicts behavior similar to that observed experimentally, that is, *a* and *b* decrease, and *c* increases as temperature in the ferromagnetic region increases. Despite a single magnetoelastic parameter used in the calculations, the model also predicts that

stress components are dependent on magnetization through the magnetic moment components, $\langle J^i \rangle$, as can be seen from equations (8)-(10).

Considering that the model contains two parameters, namely, the exchange interactions parameter without strain (λ_0) and the z-axis magnetoelastic interactions parameter (λ_{31}), it can be further reduced to a single free variable. Recall that GdNi undergoes a second-order magnetic phase transition, hence, its Curie temperature (T_C) is independent of the magnetoelastic interactions [12,42]. This allows one to fix $\lambda_0 = 1.148$ meV to properly reproduce experimentally observed $T_C = 70$ K, and still describe both the temperature-dependent lattice parameters and the magnetic properties of this compound, leaving λ_{31} a single adjustable parameter. The latter is selected for best fit of the modelled functions using experimental data for the lattice parameters and heat capacity [13]. As a result, we find $\lambda_{31} = -32$ meV and -25.5 meV for, respectively, the first and second sets of the stiffness constants of Table 2.

Figure 1 shows the temperature dependencies of the lattice parameters of GdNi, where the values calculated using the second set of parameters from Table 2 are compared with the experimental lattice parameters from Ref. [13]. Theoretical results of Figure 1 were obtained considering the thermal expansion of the lattice parameters explicitly, for example, for a as:

$$a(T) = a_0 + a_0\varepsilon_1(T, \mu_0 H) + a_0\alpha_1 T, \tag{12}$$

where a_0 and α_1 are, respectively, the y-axis intercept (a at 0 K) and the slope (thermal expansion coefficient) of the linear fit of the experimental data for the lattice parameter a above T_C, and $\varepsilon_1(T, \mu_0 H)$ is given by equation (8). The relations for $b(T)$ and $c(T)$ are similar, with a_0 and α_1, b_0 and α_2, and c_0 and α_3 listed in Table 4 y-axis intercepts and thermal expansion coefficients obtained from linear fits of the experimental data from ref. [13] in the paramagnetic region.

Table 4: y-axis intercepts and thermal expansion coefficients obtained from linear fits of the experimental data from ref. [13] in the paramagnetic region.

a_0 (Å)	b_0 (Å)	c_0 (Å)	$\alpha_1 (K^{-1})$	$\alpha_2 (K^{-1})$	$\alpha_3 (K^{-1})$
3.755	10.245	4.246	13.978×10^{-6}	24.038×10^{-6}	0

One can see a good agreement between the theoretical results and experimental data for the $a(T)$ and $c(T)$, whereas the calculated values for $b(T)$ are underestimated in the ferromagnetic region. An increase of the magnetoelastic parameter improves the $b(T)$ results but the agreement for $a(T)$ and $c(T)$ deteriorates, leading to overvaluations in the ferromagnetic region. Similar results are obtained when the first set of parameters from Table 1 is used in calculations (not shown).
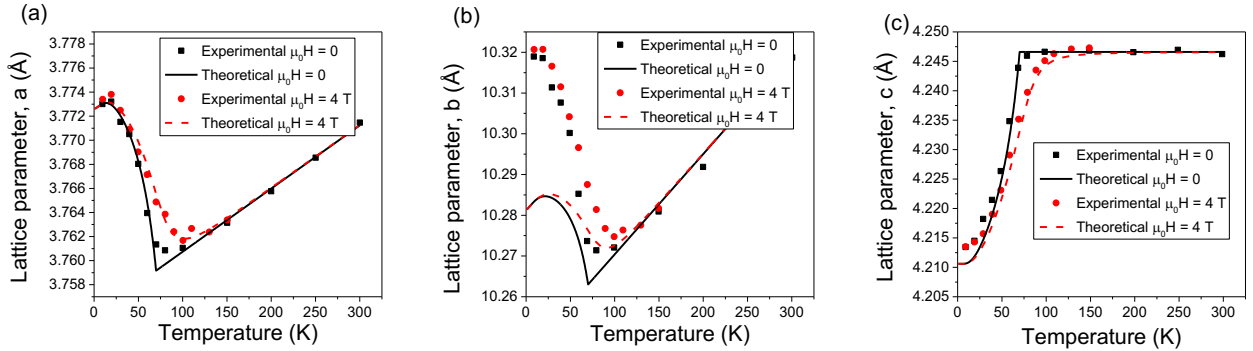
Figure 1: Temperature dependencies of lattice parameters of GdNi. Solid and dashed lines represent theoretical calculations and symbols are experimental data [13].

Figure 2(a) shows the heat capacity of GdNi for $\mu_0 H = 0$, 2 and 5 T. The symbols represent experimental data [13] and lines are theoretical results for the second set of parameters of Table 1. In order to calculate heat capacity, we added the lattice contribution to the magnetic heat capacity derived from the model. The lattice heat capacity was calculated in the Debye approximation with $\Theta_D = 200\ K$, very close to the value obtained from the DFT calculations of Table 3. The electronic contribution to the heat capacity

is neglected because it is much smaller when compared to the lattice and magnetic contributions around T_C.

One may note a good agreement between the experimental data and the theoretical results.

Figure 2(b) shows a comparison between experimental data and theoretical calculations using the first and second set of parameters of Table 1, as well as the capacity calculated without accounting for magnetoelastic interactions. Clearly, including the magnetoelastic interactions leads to a much better representation of the experimental heat capacity, both in the shape and values of the heat capacity around T_C. One can also observe a slightly better fit for the $4f$ as core electrons (second set) of the calculated parameters. This is because the magnetoelastic parameter for the $4f$ as core electrons calculations is slightly smaller than the magnetoelastic parameter for the 4f as valence electrons (first set), which results in a smoother transition and smaller values of the heat capacity around the Curie temperature.

Notably, these results indicate that $4f$ as core electrons approximation may be used to obtain elastic constants of a broader family of Gd-based intermetallics, and these constants may be later used in model Hamiltonians to describe, for instance, anisotropic behaviors of lattice parameters. We also note that treating $4f$ as core electrons decreases the computational effort in DFT, since more complicated than a simple ferromagnet magnetic structures (e.g., an antiferromagnetic one) do not need to be explicitly considered during the simulations. This conclusion is in line with previous analysis of rare earth-based materials that consider the $4f$ electrons as core, see for instance [43,44].
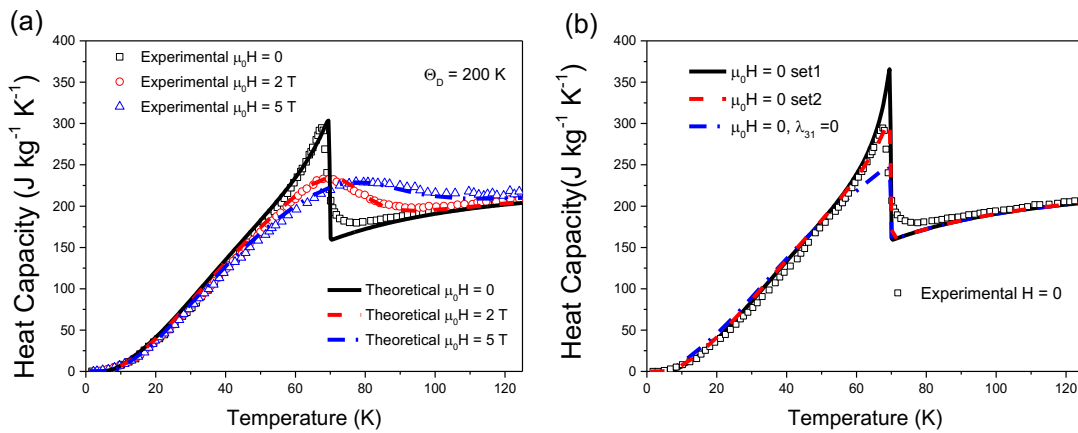
Figure 2: Temperature dependence of the GdNi heat capacity in zero and applied magnetic fields of 2 and 5 T (a). (b) Comparison between zero-field heat capacity of GdNi and theoretical results assuming $4f$ as

12

valence (set 1) and 4f as core (set 2) electrons, and neglecting magnetoelastic interactions. Lines represent computed results and symbols represent experimental data of Ref. [13].

Figure 3(a) shows the temperature dependence of the isothermal entropy change, ΔS_T, and Fig. 3(b) is the same for the adiabatic temperature change, ΔT_S, for magnetic field changes from 0 to 2 T and 0 to 5 T. The theoretically calculated magnetocaloric effect is higher when compared to the experimentally available data for ΔS_T [15] and ΔT_S, with the latter calculated from the entropies derived from experimental $C_p(T)$ data of [13] using $S = \int \frac{C_p}{T} dT$. The discrepancies are expected because in addition to assumptions and simplifications explained above, the experimental data are obtained from a polycrystalline sample and the theoretical results are obtained by assuming a single crystal [45]. When comparing the ΔS_T results calculated with and without the magnetoelastic interaction parameter, as shown in Figure 4, the shapes of the $\Delta S_T(T)$ curves more closely follow experimental results at temperatures below T_C when the strain due to ferromagnetic ordering becomes significant. This is highlighted in the inset of Figure 4 illustrating $\Delta S_T(T)$ data normalized to the corresponding peak values.
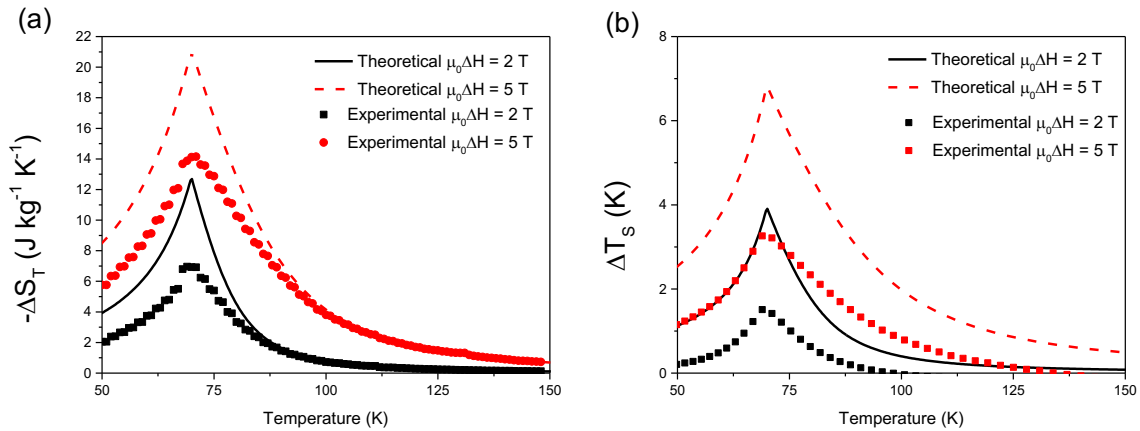
Figure 3: (a) Isothermal entropy change and (b) adiabatic temperature change of GdNi as functions of temperature under magnetic field changes from 0 to 2 and 0 to 5 T. Lines represent the results of model calculations and symbols represent values calculated from the experimental data shown in Figure 2 [13,15].
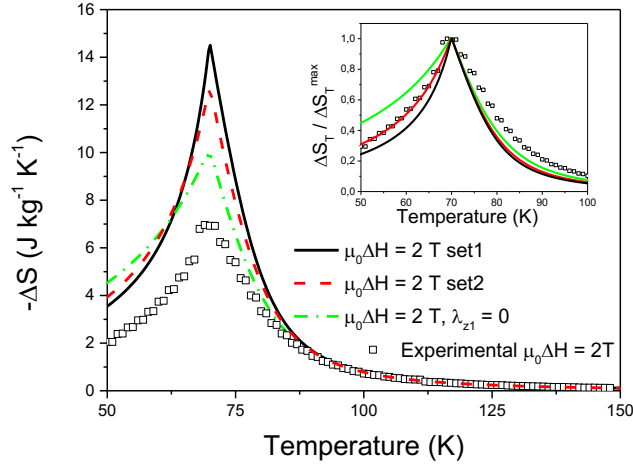
Figure 4: Comparison of the isothermal entropy change of GdNi computed from the model with and without magnetoelastic interactions. Inset shows same data normalized to the corresponding peak values. Lines represent model calculations while symbols are from experimental heat capacity data of Fig. 2 [15].

5. Final comments

In summary, we introduce a model Hamiltonian that includes coupling of anisotropic magnetoelastic interactions and magnetic degrees of freedom in addition to exchange and Zeeman terms. The model, reduced to a single adjustable variable, reproduces anisotropic changes of lattice parameters and specific heat in zero and applied magnetic fields, as well as magnetocaloric effect of GdNi qualitatively, and for some properties, nearly quantitatively. An excellent agreement between measured and calculated specific heat indicates that treating $4f$ electrons of Gd as core electrons and using DFT-derived stiffness constants as inputs into the mean-field Hamiltonian is a viable approach. This approach likely opens door to predictions of stiffness constants and temperature- and field-dependent magnetoelastic behaviors in other rare-earth materials where magnetic structures may be different from a simple ferromagnetic arrangement of the magnetic moments. We also hope that the results of this work will lead to applying the same methodology to investigate other compounds known to exhibit anisotropic temperature dependencies of lattice parameters in the magnetically-ordered state, such as antiferromagnetic $GdNiSi_3$ [14].

Acknowledgments

References

[1]   N.D. Mathur, F.M. Grosche, S.R. Julian, I.R. Walker, D.M. Freye, R.K.W. Haselwimmer, G.G. Lonzarich, Magnetically mediated superconductivity in heavy fermion compounds, Nature. 394, 39–43 (1998). https://doi.org/10.1038/27838.

[2]   X.F. Wang, X.G. Luo, J.J. Ying, Z.J. Xiang, S.L. Zhang, R.R. Zhang, Y.H. Zhang, Y.J. Yan, A.F. Wang, P. Cheng, G.J. Ye, X.H. Chen, Enhanced superconductivity by rare-earth metal doping in phenanthrene, J. Phys. Condens. Matter. 24, 345701 (2012). https://doi.org/10.1088/0953-8984/24/34/345701.

[3]   V.K. Pecharsky, K.A. Gschneidner, Giant magnetocaloric effect in $Gd_5(Si_2Ge_2)$, Phys. Rev. Lett. 78, 4494–4497 (1997). https://doi.org/10.1103/PhysRevLett.78.4494.

[4]   J. V. Alvarez, H. Rieger, A. Zheludev, Dilution-Controlled Quantum Criticality in Rare-Earth Nickelates, Phys. Rev. Lett. 93, 156401 (2004). https://doi.org/10.1103/PhysRevLett.93.156401.

[5]   F. Guillou, A.K. Pathak, D. Paudyal, Y. Mudryk, F. Wilhelm, A. Rogalev, V.K. Pecharsky, Non-hysteretic first-order phase transition with large latent heat and giant low-field magnetocaloric effect, Nat. Commun. 9, 2925 (2018). https://doi.org/10.1038/s41467-018-05268-4.

[6]   A. Biswas, N.A. Zarkevich, A.K. Pathak, O. Dolotko, I.Z. Hlova, A. V. Smirnov, Y. Mudryk, D.D. Johnson, V.K. Pecharsky, First-order magnetic phase transition in Pr_2In with negligible thermomagnetic hysteresis, Phys. Rev. B. 101, 224402 (2020). https://doi.org/10.1103/PhysRevB.101.224402.

[7]   P.O. Ribeiro, B.P. Alho, T.S.T. Alvarenga, E.P. Nóbrega, A.M.G. Carvalho, V.S.R. de Sousa, A. Caldas, N.A. de Oliveira, P.J. von Ranke, Theoretical investigations on the magnetocaloric and barocaloric effects in TbyGd(1−y)Al2 series, J. Alloys Compd. 563, 242–248 (2013). https://doi.org/10.1016/j.jallcom.2013.02.068.

[8]   P.J. von Ranke, T.S.T. Alvarenga, B.P. Alho, E.P. Nóbrega, P.O. Ribeiro, A.M.G. Carvalho, V.S.R. de Sousa, A. Caldas, N.A. de Oliveira, Spin reorientation and the magnetocaloric effect in $Ho_yEr_{(1−y)}N$, J. Appl. Phys. 111, 113916 (2012). https://doi.org/10.1063/1.4728201.

[9]   T.S.T. Alvaranega, B.P. Alho, E.P. Nobrega, P.O. Ribeiro, A. Caldas, V.S.R. de Sousa, A. Magnus, G. Carvalho, N.A. de Oliveira, P.J. von Ranke, Theoretical investigation on the barocaloric and magnetocaloric properties in the $Gd_5Si_2Ge_2$ compound, J. Appl. Phys. 116, 243908 (2014). https://doi.org/10.1063/1.4904959.

[10]   C.P. Bean, D.S. Rodbell, Magnetic Disorder as a First-Order Phase Transformation, Phys. Rev. 126, 104–115 (1962). https://doi.org/10.1103/PhysRev.126.104.

[11]   E. Mendive-Tapia, D. Paudyal, L. Petit, J.B. Staunton, First-order ferromagnetic transitions of lanthanide local moments in divalent compounds: An itinerant electron positive feedback mechanism and Fermi surface topological change, Phys. Rev. B. 101, 174437 (2020). https://doi.org/10.1103/PhysRevB.101.174437.

[12]   B.P. Alho, P.O. Ribeiro, P.J. von Ranke, F. Guillou, Y. Mudryk, V.K. Pecharsky, Free-energy analysis of the nonhysteretic first-order phase transition of Eu_2In, Phys. Rev. B. 102, 134425 (2020). https://doi.org/10.1103/PhysRevB.102.134425.

[13]   D. Paudyal, Y. Mudryk, Y.B. Lee, V.K. Pecharsky, K.A. Gschneidner, B.N. Harmon, Understanding the extraordinary magnetoelastic behavior in GdNi, Phys. Rev. B. 78, 184436 (2020). https://doi.org/10.1103/PhysRevB.78.184436.

[14]   R. Tartaglia, F.R. Arantes, C.W. Galdino, D. Rigitano, U.F. Kaneko, M.A. Avila, E. Granado, Magnetic structure and magnetoelastic coupling of $GdNiSi_3$ and $TbNiSi_3$, Phys. Rev. B. 99, 094428 (2019). https://doi.org/10.1103/PhysRevB.99.094428.

[15]   A. Biswas, T. Del Rose, Y. Mudryk, P.O. Ribeiro, B.P. Alho, V.S.R. de Sousa, E.P. Nóbrega, P.J. von Ranke, V.K. Pecharsky, Hidden first-order phase transitions and large magnetocaloric effects in $GdNi_{1-x}Co_x$, J. Alloys Compd. 897, 163186 (2022). https://doi.org/10.1016/j.jallcom.2021.163186.

[16]   R.E. Walline, W.E. Wallace, Magnetic and Structural Characteristics of Lanthanide—Nickel Compounds, J. Chem. Phys. 41, 1587–1591 (1964). https://doi.org/10.1063/1.1726127.

[17]   S.C. Abrahams, J.L. Bernstein, R.C. Sherwood, J.H. Wernick, H.J. Williams, The crystal structure and magnetic properties of the rare-earth nickel (RNi) compounds, J. Phys. Chem. Solids. 25, 1069–1080 (1964). https://doi.org/10.1016/0022-3697(64)90129-5.

[18]   W. Voigt, Lehrbuch Der Kristallphysik, Vieweg teubner Verlag, 1928.

[19]   G.R. Barsch, Relation between Third-Order Elastic Constants of Single Crystals and Polycrystals, J. Appl. Phys. 39, 3780–3793 (1968). https://doi.org/10.1063/1.1656855.

[20]   L.D. Landau, E.M. Lifshitz, Theory of Elasticity, Elsevier, 1986. https://doi.org/10.1016/C2009-0-25521-8.

[21]   P.J. von Ranke, N.A. de Oliveira, C. Mello, A.M.G. Carvalho, S. Gama, Analytical model to understand the colossal magnetocaloric effect, Phys. Rev. B. 71, 054410 (2005). https://doi.org/10.1103/PhysRevB.71.054410.

[22]   P. Giannozzi, S. Baroni, N. Bonini, M. Calandra, R. Car, C. Cavazzoni, D. Ceresoli, G.L. Chiarotti, M. Cococcioni, I. Dabo, A. Dal Corso, S. de Gironcoli, S. Fabris, G. Fratesi, R. Gebauer, U. Gerstmann, C. Gougoussis, A. Kokalj, M. Lazzeri, L. Martin-Samos, N. Marzari, F. Mauri, R. Mazzarello, S. Paolini, A. Pasquarello, L. Paulatto, C. Sbraccia, S. Scandolo, G. Sclauzero, A.P. Seitsonen, A. Smogunov, P. Umari, R.M. Wentzcovitch, QUANTUM ESPRESSO: a modular and open-source software project for quantum simulations of materials, J. Phys. Condens. Matter. 21, 395502 (2009). https://doi.org/10.1088/0953-8984/21/39/395502.

[23]   P. Giannozzi, O. Andreussi, T. Brumme, O. Bunau, M. Buongiorno Nardelli, M. Calandra, R. Car, C. Cavazzoni, D. Ceresoli, M. Cococcioni, N. Colonna, I. Carnimeo, A. Dal Corso, S. de Gironcoli, P. Delugas, R.A. DiStasio, A. Ferretti, A. Floris, G. Fratesi, G. Fugallo, R. Gebauer, U. Gerstmann, F. Giustino, T. Gorni, J. Jia, M. Kawamura, H.-Y. Ko, A. Kokalj, E. Küçükbenli, M. Lazzeri, M. Marsili, N. Marzari, F. Mauri, N.L. Nguyen, H.-V. Nguyen, A. Otero-de-la-Roza, L. Paulatto, S. Poncé, D. Rocca, R. Sabatini, B. Santra, M. Schlipf, A.P. Seitsonen, A. Smogunov, I. Timrov, T. Thonhauser, P. Umari, N. Vast, X. Wu, S. Baroni, Advanced capabilities for materials modelling with Quantum ESPRESSO, J. Phys. Condens. Matter. 29, 465901 (2017). https://doi.org/10.1088/1361-648X/aa8f79.

[24]   P. Giannozzi, O. Baseggio, P. Bonfà, D. Brunato, R. Car, I. Carnimeo, C. Cavazzoni, S. de Gironcoli, P. Delugas, F. Ferrari Ruffino, A. Ferretti, N. Marzari, I. Timrov, A. Urru, S. Baroni,

Quantum ESPRESSO toward the exascale, J. Chem. Phys. 152, 154105 (2020). https://doi.org/10.1063/5.0005082.

[25]   Quantum ESPRESSO. https://github.com/dalcorso/thermo_pw.

[26]   K. Lejaeghere, G. Bihlmayer, T. Björkman, P. Blaha, S. Blügel, V. Blum, D. Caliste, I.E. Castelli, S.J. Clark, A. Dal Corso, S. De Gironcoli, T. Deutsch, J.K. Dewhurst, I. Di Marco, C. Draxl, M. Dułak, O. Eriksson, J.A. Flores-Livas, K.F. Garrity, L. Genovese, P. Giannozzi, M. Giantomassi, S. Goedecker, X. Gonze, O. Grånäs, E.K.U. Gross, A. Gulans, F. Gygi, D.R. Hamann, P.J. Hasnip, N.A.W. Holzwarth, D. Iuşan, D.B. Jochym, F. Jollet, D. Jones, G. Kresse, K. Koepernik, E. Küçükbenli, Y.O. Kvashnin, I.L.M. Locht, S. Lubeck, M. Marsman, N. Marzari, U. Nitzsche, L. Nordström, T. Ozaki, L. Paulatto, C.J. Pickard, W. Poelmans, M.I.J. Probert, K. Refson, M. Richter, G.M. Rignanese, S. Saha, M. Scheffler, M. Schlipf, K. Schwarz, S. Sharma, F. Tavazza, P. Thunström, A. Tkatchenko, M. Torrent, D. Vanderbilt, M.J. Van Setten, V. Van Speybroeck, J.M. Wills, J.R. Yates, G.X. Zhang, S. Cottenier, Reproducibility in density functional theory calculations of solids, Science. 351 (2016). https://doi.org/10.1126/science.aad3000.

[27]   G. Prandini, A. Marrazzo, I.E. Castelli, N. Mounet, N. Marzari, Precision and efficiency in solid-state pseudopotential calculations, Npj Comput. Mater. 4, 72 (2018). https://doi.org/10.1038/s41524-018-0127-2.

[28]   M. Topsakal, R.M. Wentzcovitch, Accurate projected augmented wave (PAW) datasets for rare-earth elements (RE=La–Lu), Comput. Mater. Sci. 95, 263–270 (2018). https://doi.org/10.1016/j.commatsci.2014.07.030.

[29]   A. Dal Corso, Pseudopotentials periodic table: From H to Pu, Comput. Mater. Sci. 95, 337–350 (2014). https://doi.org/10.1016/j.commatsci.2014.07.043.

[30]   K.F. Garrity, J.W. Bennett, K.M. Rabe, D. Vanderbilt, Pseudopotentials for high-throughput DFT calculations, Comput. Mater. Sci. 81, 446–452 (2014). https://doi.org/10.1016/j.commatsci.2013.08.053.

[31]   J.P. Perdew, K. Burke, M. Ernzerhof, Generalized Gradient Approximation Made Simple, Phys. Rev. Lett. 77, 3865–3868 (1996). https://doi.org/10.1103/PhysRevLett.77.3865.

[32]   J.P. Perdew, K. Burke, M. Ernzerhof, Generalized Gradient Approximation Made Simple [Phys. Rev. Lett. 77, 3865 (1996)], Phys. Rev. Lett. 78, 1396–1396 (1997). https://doi.org/10.1103/PhysRevLett.78.1396.

[33]   M. Cococcioni, S. de Gironcoli, Linear response approach to the calculation of the effective interaction parameters in the LDA+U method, Phys. Rev. B. 71, 035105 (2005). https://doi.org/10.1103/PhysRevB.71.035105.

[34]   F. Birch, Finite Elastic Strain of Cubic Crystals, Phys. Rev. 71, 809–824 (1947). https://doi.org/10.1103/PhysRev.71.809.

[35]   F.D. Murnaghan, The Compressibility of Media under Extreme Pressures, Proc. Natl. Acad. Sci. 30, 244–247 (1944). https://doi.org/10.1073/pnas.30.9.244.

[36]   M. Methfessel, A.T. Paxton, High-precision sampling for Brillouin-zone integration in metals, Phys. Rev. B. 40, 3616–3621 (1989). https://doi.org/10.1103/PhysRevB.40.3616.

[37] F. Mouhat, F.-X. Coudert, Necessary and sufficient elastic stability conditions in various crystal systems, Phys. Rev. B. 90, 224104 (2014). https://doi.org/10.1103/PhysRevB.90.224104.

[38] A. Reuss, Berechnung der Fließgrenze von Mischkristallen auf Grund der Plastizitätsbedingung für Einkristalle ., ZAMM - Zeitschrift Für Angew. Math. Und Mech. 9, 49–58 (1929). https://doi.org/10.1002/zamm.19290090104.

[39] R. Hill, The Elastic Behaviour of a Crystalline Aggregate, Proc. Phys. Soc. Sect. A. 65, 349–354 (1952). https://doi.org/10.1088/0370-1298/65/5/307.

[40] O.L. Anderson, A simplified method for calculating the debye temperature from elastic constants, J. Phys. Chem. Solids. 24, 909–917 (1963). https://doi.org/10.1016/0022-3697(63)90067-2.

[41] P. Ravindran, L. Fast, P.A. Korzhavyi, B. Johansson, J. Wills, O. Eriksson, Density functional theory for calculation of elastic properties of orthorhombic crystals: Application to $TiSi_2$, J. Appl. Phys. 84, 4891–4904 (1998). https://doi.org/10.1063/1.368733.

[42] B.P. Alho, N.A. de Oliveira, V.S.R. de Sousa, S. Gama, A.A. Coelho, A.M.G. Carvalho, P.J. von Ranke, Theoretical investigation on the magnetocaloric effect in MnAs using a microscopic model to describe the magnetic and thermal hysteresis, Solid State Commun. 152, 951–954 (2012). https://doi.org/10.1016/j.ssc.2012.03.028.

[43] S. Coh, T. Heeg, J.H. Haeni, M.D. Biegalski, J. Lettieri, L.F. Edge, K.E. O'Brien, M. Bernhagen, P. Reiche, R. Uecker, S. Trolier-McKinstry, D.G. Schlom, D. Vanderbilt, Si-compatible candidates for high-k dielectrics with the Pbnm perovskite structure, Phys. Rev. B. 82, 064101 (2010). https://doi.org/10.1103/PhysRevB.82.064101.

[44] M. Topsakal, C. Leighton, R.M. Wentzcovitch, First-principles study of crystal and electronic structure of rare-earth cobaltites, J. Appl. Phys. 119, 244310 (2016). https://doi.org/10.1063/1.4954792.

[45] P.O. Ribeiro, B.P. Alho, R.S. De Oliveira, E.P. Nóbrega, V.S.R. de Sousa, P.J. von Ranke, A. Biswas, M. Khan, Y. Mudryk, V.K. Pecharsky, Magnetothermal properties of $Ho_{1-x}Dy_xAl_2$ (x = 0, 0.05, 0.10, 0.15, 0.25 and 0.50) compounds, J. Magn. Magn. Mater. 544, 168705 (2016). https://doi.org/10.1016/j.jmmm.2021.168705.